Supporting Information

Vizcarra et al. 10.1073/pnas.1105703108

SI Discussion

Affinity Measurements. The affinity of Capu-tail for Dm-kinase noncatalytic C-lobe domain (KIND) reported in the text (290 nM) is derived from fitting the competition curve for the anisotropy of 10 nM Capu-tail-AlexaFluor488, 800 nM KIND, and varying concentrations of unlabeled Capu-tail. This is similar to the K_d value of 260 nM, derived for hSpir1-KIND and an extended version of mFmn2-tail from a competition experiment (1). The tighter affinity measured for the unlabeled tail peptides and KIND (140 nM) indicate that the dye contributes to the binding affinities shown in Fig. S3 and listed in Table S1. However, we expect that the relative effects of point-mutations are independent of the attached fluorophore. This is confirmed for a subset of mutations using pyrene actin assembly assays shown in Fig. S3*D* and in vivo colocalization studies (Fig. 4 and Fig. S6). The Dm-Spir-KIND single mutations fall into three groups based on their affinities for the Capu-tail: those that had a small to negligible effect on binding (E226A, T233A, E241A, E244A), those that have an intermediate effect (E229K, D236A/N, E252A), and strong mutations (Y232A/K).

The functional competition experiment (Fig. 1*B*) can also be interpreted as a measure of Capu-tail affinity for KIND. Analysis of competition binding is well described in Vinson et al. (2). Accordingly, the fraction of protein bound (in this case Capu-CT bound to KIND in the presence of competing Capu-tail) is given by

$$f = \frac{1}{K_d(\frac{L+K_{d2}}{K_{d2}R_0}) + 1},$$

where $L = [\text{Capu-tail}]$, $R_0 = [\text{KIND}]$, $K_d =$ the affinity of Capu-CT for KIND and $K_{d2} =$ the affinity of Capu-tail for KIND. At $f = 0.5$, if $K_d = K_{d2}$, this equation reduces to $L = R_0 - K_d$. We previously reported that under these conditions Capu-CT binds KIND with a $K_d = 5$ nM (3). Thus L should be close to R_0 (800 nM) in our experiment. We observed a half-maximal response at approximately 1 μM (L) of the peptide, close to the concentration of Spir-KIND present, suggesting that the Capu-tail and Capu-CT bind Dm-Spir-KIND with similar affinities.

Stoichiometry of the Spir/Fmn Complex. Previous analyses of the stoichiometry of the Spir/Capu complex yielded conflicting results: sedimentation equilibrium experiments gave a molecular weight for the complex that was consistent with two KIND domains per FH2 dimer for *Drosophila* isoforms (3), whereas analytical gel-filtration data indicated that there was just one KIND domain per FH2 dimer for mammalian isoforms (1). We do not expect that the stoichiometry is species-specific and therefore, revisited this question. Previously reported functional data also points to a 2:2 stoichiometry: the actin assembly activity of Spir-NT (containing both the KIND and four WH2 domains) is enhanced by the addition of a nucleation-incompetent Capu-CT. The maximal rate of assembly is observed at one Capu-CT subunit per Spir-NT and decreases with additional Capu-CT (3). The enhanced activity was hypothesized to be an effect of dimerizing Spir, creating a nucleator with eight WH2 domains as opposed to four. To further test this hypothesis, we created an artificially dimerized Spir-NT using a GST-tag. GST-Spir-NT has enhanced nucleation activity, similar to the effect observed when nucleation-incompetent Capu-CT is added to monomeric Spir-NT (Fig. S2*G*).

We then used a second absolute (i.e., independent of standards) means of measuring the molecular weight of the complex to determine the stoichiometry. Size-exclusion chromatography coupled to multiangle light scattering (SEC-MALS) was carried out on the human isoforms of KIND and FH2C (Fig. S2*H*). When Fmn2-FH2C was analyzed in the presence of a slight excess of KIND a peak with molecular weight of 150 kDa eluted, in good agreement with the predicted molecular weight (146 kDa) for two KIND domains per Fmn2-FH2C dimer. The stoichiometry was further confirmed by quantitative gel analysis of this peak. Note that the size-exclusion chromatography was carried out with 1.7 μM Spir1-KIND domain in the gel-filtration buffer. Our analysis here suggests that the previous study by gel-filtration underestimated the stoichiometry of the complex due to partial dissociation of the complex on the column, which is not unexpected given the modest affinity of the interaction. Inclusion of free Spir-KIND domain in the gel-filtration buffer (at a concentration approximately tenfold above the K_d) allows accurate analysis of the mass and stoichiometry by SEC-MALS as we describe here. Finally, the structural models that we determined using X-ray crystallography show a complex with one KIND monomer per tail, which is consistent with two KIND monomers per FH2 dimer. Therefore we conclude that two Spir-KIND domains are bound to the formin dimer.

Capu-CT Association with Filament Barbed Ends. Capu-CT (Fig. S7*D*, light blue trace) modestly increases the assembly rate from preformed seeds compared to the G-actin plus seeds (gray trace). We hypothesize that the increase in elongation rate in the presence of Capu-CT is due to a low level of nucleation of new filaments by Capu under these conditions because (*i*) there was a small enhancement of actin assembly by Capu in assembly reactions lacking preformed seeds (Fig. S7*F*, *Inset*), and (*ii*) in the presence of profilin, the assembly rate from seeds was the same with or without Capu (Fig. S7*F*). A decreased rate of barbed end depolymerization and decreased filament annealing in the presence of Capu could also contribute to this affect. Direct, single-filament observation will be necessary to determine the exact rate of elongation for Capu-bound filaments.

Both elongation assays and filament annealing assays suggest that the KIND domain competes with barbed ends for Capu-CT binding. We observe that the preformed complex is unlikely to bind to filament ends, whether growing or static, and that the KIND domain can actually knock Capu-CT off of filament ends. These distinct conclusions come from the order of addition of proteins in both assays. When Capu-CT and KIND are mixed before being introduced to actin, growing filaments are not protected from capping protein (Fig. 5*A*, +Capu-CT+KIND+CP) and reannealing proceeds more than in the absence of KIND (Fig. 5*B*). When Capu-CT is mixed with filaments before addition of KIND, the results are the same (Fig. S7*E* and Fig. 5*B*). In filament annealing assays, filament lengths do not recover to the extent that they do in the absence of Capu-CT regardless of order of addition, suggesting that there is competition between filaments ends and KIND for Capu-CT binding. This assay is more sensitive than the elongation assay, which shows complete inhibition of elongation after addition of KIND, because it reports a condition closer to equilibrium between only these three players. In the case of the elongation assay, capping protein caps so potently that when Capu-CT comes off a filament it cannot bind again whether or not it is associated with KIND. These data allow us to eliminate one of the models of Spir/Capu interaction in which they remain associated with growing filament ends (4).

Mechanism in Context of Oogenesis. Our discovery of a role for the Capu-tail in actin nucleation suggests an explanation for the observation that exogenous expression of Capu can rescue *spir* null mutants in the fly (5). If the Capu-tail indeed participates in nucleation by binding actin monomers, Spir may enhance nucleation by effectively replacing this activity with the more robust, tetravalent actin binding of its WH2 array. Thus overexpression of Capu can rescue *spir* mutants because it provides the requisite elements for nucleation and processive capping. The converse is not true; whereas Spir alone may nucleate filaments, it does not have processive capping activity.

There is conflicting evidence in the field regarding barbed versus pointed end binding by Spir alone (6–8). Our data do not directly address this issue. Instead, they suggest that irrespective of which end Spir binds, release of the KIND/tail interaction likely needs to occur for the formin to processively cap new filaments.

SI Methods.

Expression and Purification of Spir1, Fmn1, and Fmn2 Proteins for GST Pull-Down Assays. A His_6-Spir1 (aa 20–237; based on Genbank entry NM_020148) construct was generated in a pET vector (Novagen) by standard PCR amplification of cDNA and subcloning methods. Fragments of human Fmn1 or Fmn2 cDNA were amplified from placental mRNA by RT-PCR (Clontech). Tail segments of human Fmn2 (aa 1700–1722) or Fmn1 (aa 1167–1196; based on GenBank entry NM_001103184) were amplified by PCR and subcloned into a modified pET vector directing expression of N-terminal GST-fusion proteins. These constructs were transformed in *Escherichia coli* BL21(DE3) and cultured in 800 mL LB media until an OD_{600} of 0.6 was reached. Expression was induced by adding 200 μM isopropyl-β-D-thiogalactopyranoside (IPTG) and shaking for 18–20 h at 18 °C. Cells were harvested by centrifugation and each pellet was resuspended in 15 mL of 25 mM Tris-HCl pH 8.0, 200 mM NaCl.

His_6-Spir1 KIND domain was purified by Ni-NTA agarose by the following procedure. Pellets were handled on ice using ice-cold buffers. Pellets were diluted 2-fold with 25 mM Tris-HCl, 10 mM β-mercaptoethanol (βME), 200 mM NaCl, 50 mM imidazole, and lysed by homogenization at 30,000 psi at 10 °C (Constant Systems). The lysate was centrifuged at 40,000 × *g*, 40 min, 4 °C, and the resulting supernatant was filtered with MILLEX GV syringe-driven PVDF filters (Millipore). The clarified lysate was mixed with 4 mL of Ni-NTA agarose preequilibrated in 25 mM Tris-HCl pH 8.0, 5 mM βME, 200 mM NaCl, 25 mM imidazole, and incubated for 1–2 h at 4 °C with gentle end-over-end mixing in a closed column. Following flow-through of unbound proteins, the resin was washed with 25 column volumes (cv) of 25 mM Tris-HCl pH 8.0, 5 mM βME, 300 mM NaCl, 25 mM imidazole, and His_6-Spir1 KIND domain protein was eluted in 5 fractions of 8 mL of 25 mM Tris-HCl pH 8.0, 5 mM βME, 100 mM NaCl, 400 mM imidazole. Peak fractions were pooled, supplemented with 2 mM tris(2-carboxyethyl)phosphine (TCEP), and concentrated in Amicon Ultra-15 concentrator units (10,000 Da cutoff; Millipore). The concentrated protein was then diluted to approximately 10 mg/mL with buffer A (25 mM Tris-HCl pH 8.0, 2 mM TCEP, 100 mM NaCl), centrifuged at 15,000 × *g* for 10 min at 4 °C to remove any particulates, then loaded onto a Superdex S200 10/30 gel-filtration column equilibrated in buffer A. Peak fractions containing His_6-Spir1 KIND were pooled and concentrated by ultrafiltration as described above.

GST-Fmn1 or GST-Fmn2 expression pellets were each diluted with 25 mM Tris-HCl pH 8.0, 200 mM NaCl to a total volume of 45 mL, supplemented with 2 mM TCEP, and mixed gently. Cell lysates were prepared and clarified as described above for His_6-Spir1 KIND domain. The clarified lysate was mixed with glutathione sepharose 4 fast-flow resin for 3 h at 4 °C with gentle rocking in a closed column. Following flow-through of unbound proteins, the resin was washed with 20 cv of 25 mM Tris-HCl pH 8.0, 2 mM TCEP, 300 mM NaCl then 2 cv of buffer A. Finally, beads were resuspended as a 50% slurry in buffer A for inclusion in pull-down experiments.

Expression and Purification of Spir and Capu Proteins for Anisotropy and Actin Polymerization Measurements. The wild-type (WT) and mutant tail domains of Capu (aa 1029–1059) were expressed as N-terminal GST fusions using the vector pGEX-6P-2 (GE Healthcare). WT and mutant KIND domains (aa 1–327 of *Drosophila melanogaster* Spire) were expressed with a C-terminal His_6 tag in the vector pET20b(+). Capu-CT mutants (aa 467–1059) and truncations were expressed with an N-terminal His_6 tag in the vector pQE80L or in a modified version of pET15b. Spir-NT (aa 1–490) was purified using an internal poly His sequence as an affinity tag. For Dm-Spir-KIND domains and Capu-tail constructs, expression was induced in *E. coli* BL21(DE3) pLysS cells by addition of 250 μM IPTG and shaking for 3 h at 37 °C. Capu-CT proteins were expressed using *E. coli* Rosetta™(DE3) cells (EMD Biosciences), and were induced by addition of 250 μM IPTG and shaking overnight at 20 °C. Spir-NT (aa 1–490) was expressed using BL21(DE3) pLysS cells by addition of 250 μM IPTG and shaking overnight at 18 °C. All proteins were expressed using Terrific Broth medium supplemented with 100 mg/L ampicillin and, for Rosetta cell cultures, 32 mg/L chloramphenicol. Bacteria were harvested by centrifugation, pellets were washed once with ice-cold PBS, and frozen at −80 °C. All purification steps were carried out at 4 °C. Thawed cells were diluted at least twofold with lysis buffer supplemented with 1 mM phenylmethylsulfonyl fluoride (PMSF) and 2 μg/mL DNaseI and then lysed by microfluidizing. Cell debris was removed by centrifugation at 20,000 × *g* for 20 min at 4 °C. Clarified lysates were then nutated with either glutathione sepharose or TALON (R) resin (Clontech) for 1 h at 4 °C.

For all GST-Capu-tail fusions, the resin was washed with 20 cv of the same PBS in which the cells were lysed [140 nM $CaCl_2$, 2.7 mM KCl, 10 mM sodium phosphate dibasic, 1.8 mM potassium phosphate monobasic, 1 mM 1,4-Dithiothreitol (DTT)], and proteins were eluted with 20 mM glutathione in 50 mM Tris-HCl, pH 8.0. The GST fusions were cleaved for 2–3 h with 1–5% (wt/wt) recombinant GST-tagged PreScission protease while dialyzing against PBS. The protease and cleaved GST were removed by nutating with fresh glutathione sepharose resin for 1 h. The unbound fraction was then dialyzed against 20 mM Na-Hepes pH 7.0, 1 mM DTT, 150 mM NaCl overnight, followed by 1–2 h dialysis against 20 mM Na-Hepes pH 7.0, 1 mM DTT, 100 mM NaCl. The tail constructs were further purified using an SP-FF cation exchange column (GE Life Sciences) with a gradient of 100–820 mM NaCl over 40 column volumes. Pooled fractions were dialyzed twice against 10 mM Tris-HCl pH 8.0, 150 mM NaCl, 1 mM DTT, followed by 1:1 glycerol:buffer overnight. Protein aliquots were flash-frozen in liquid nitrogen and stored at −80 °C.

His_6-tagged proteins or Spir-NT coupled to TALON (R) resin were washed with 20 cv lysis buffer (50 mM sodium phosphate pH 8.0, 1 mM βME, 300 mM NaCl), followed by washing 20 cv with 50 mM sodium phosphate pH 7.0, 1 mM βME, 300 mM NaCl. Proteins were eluted with 200 mM imidazole, 50 mM sodium phosphate pH 7.0, 1 mM βME, 300 mM NaCl, and dialyzed overnight against 10 mM Tris-HCl pH 8.0, 1 mM DTT for KIND and Capu-CT or 10 mM Hepes pH 8, 1 mM DTT for Spir-NT. These were further purified over a MonoQ anion exchange column (GE Life Sciences) using a gradient of 50–500 mM KCl over 60 cv for KIND domains, 50–250 mM KCl over 100 cv for Capu-CT, or 0–500 mM KCl over 60 cv for Spir-NT. Pooled fractions from the MonoQ column were dialyzed twice against 10 mM Tris-HCl pH 8.0, 1 mM DTT, followed by 1:1

glycerol:buffer overnight. Protein aliquots were flash-frozen in liquid nitrogen and stored at −80 °C. Tail domain concentrations were calculated by SDS-PAGE followed by quantitative SYPRO (R) Red staining using actin as a standard. KIND, Spir-NT and Capu-CT concentrations were calculated from their absorbance at 280 nm ($\varepsilon_{280} = 17452\ cm^{-1}\ M^{-1}$ for KIND, $25575\ cm^{-1}\ M^{-1}$ for Spir-NT, and $75200\ cm^{-1}\ M^{-1}$ for Capu-CT) (3).

Capu-tail(1029–1059)-KCK was expressed and purified as described above for WT Capu-tail. For labeling of Capu-tail-KCK, unlabeled protein was incubated for 30 min at 42 °C with 10 mM TCEP and then dialyzed twice for 2 h each time against 10 mM Tris-HCl pH 7.5, 100 mM KCl. Capu-tail-KCK was nutated at 25 °C for 30 min with a 1–2 molar ratio of AlexaFluor488-C5-maleimide to protein. The reaction was quenched by addition of 10 mM DTT. Unconjugated dye was removed using a PD-10 desalting column (GE Life Sciences) equilibrated with 10 mM Tris-HCl pH 8.0, 1 mM DTT, 100 mM KCl. The total concentration of protein was calculated by quantitative SYPRO (R) Red staining. The concentration of labeled protein was calculated from its absorbance at 496 nm ($\varepsilon_{496} = 71000\ cm^{-1}\ M^{-1}$). Labeling efficiencies were calculated to be greater than 99%.

Expression and Purification of the Spir1-KIND/Fmn2-tail Complex for Crystallization. His_6-Spir1 KIND (aa 20–237) and GST-Fmn2 (aa 1700–1722), each bearing tobacco etch virus (TEV) protease cleavage sites following their affinity tags, were coexpressed in *E. coli* BL21(DE3) using compatible T7-based vectors. At an OD_{600} reading of 0.6, protein expression was induced by addition of 100 μM IPTG followed by shaking for 16 h at 18 °C. Cells were harvested by centrifugation, and pellets were resuspended in lysis buffer (25 mM Tris-HCl pH 8.0, 5 mM βME, 150 mM NaCl, 25 mM imidazole). Cells were disrupted by homogenization at 30,000 psi at 10 °C. Insoluble material was removed by centrifugation at 40,000 × *g* at 4 °C for 40 min, and the soluble portion of lysate was mixed and incubated with gentle rocking with nickel (II)-chelated sepharose beads equilibrated in lysis buffer (GE Life Sciences) in a closed column. After binding at 4 °C for 1 h, the column was opened, flow-through collected, the resin was extensively washed with lysis buffer, and the complex was eluted with lysis buffer containing 400 mM imidazole. The peak eluate was then supplemented with 2 mM TCEP and incubated with glutathione sepharose 4 fast-flow resin to rebind the complex. Beads were washed with 20 column volumes of 25 mM Tris-HCl pH 8.0, 2 mM TCEP, and 150 mM NaCl, and then resuspended in 5 mL of this buffer. Higher concentrations of NaCl disrupted the complex. Recombinant His-TEV protease (0.05 mg per milligram of fusion protein) was added to remove the affinity tags from Spir1 and Fmn2 and release the free complex from the beads. The complex was further purified by gel-filtration chromatography on a Superdex 75 16/30 column equilibrated in 25 mM Tris-HCl pH 8.0, 4 mM TCEP, 100 mM NaCl. Peak fractions corresponding to the complex were pooled and concentrated to 7 mg/mL in an Amicon Ultra 15 concentrator unit (10,000 Da cutoff).

Crystallization and Structure Determination of the Spir1-KIND/Fmn2-Tail Complex. Crystallization screens of the Spir1-KIND/Fmn2-tail complex were set up in sitting drop vapor diffusion format, where 0.4 μL of protein was mixed with 0.4 μL of reservoir buffer using a Matrix Hydra II robot (Thermo Scientific). Bipyramidal crystals grew over several days at 4 °C with a reservoir solution containing 0.1 M MES pH 6.0, 5 mM TCEP, 100 mM NaCl, and 28% (vol/vol) PEG 400. These crystals belonged to space group $P4_32_12$ with unit cell dimensions $a = 66.44$ Å, $b = 66.44$ Å, and $c = 116.40$ Å and contained one copy of the Spir1-KIND/Fmn2-tail complex per asymmetric unit. To prepare heavy metal derivatives for phase determination, crystals were soaked overnight at 4 °C in a nonreducing stabilization solution containing all other components of gel-filtration buffer and reservoir solution, supplemented with an additional 2% (vol/vol) PEG 400 and either 0.25 mM ethyl mercury (II) phosphate or dipotassium platinum (II) tetrachloride.

Diffraction data were collected from crystals mounted in MicroMount assemblies (MiTeGen) at 22 °C, employing a Rigaku RU-300RC rotating anode X-ray generator with Xenocs mirrors and a Mar345dtb image plate area detector (Mar Research). Diffraction data extending to 2.2 Å or 2.4 Å were obtained from native or derivative crystals, and the phases were determined by multiple isomorphous replacement (MIR). Data were processed with HKL2000 (9), and the initial model was built using AutoSHARP (www.globalphasing.com). Waters were subsequently added with Arp/Warp (10), followed by iterative manual fitting and crystallographic refinement in the CCP4i suite (11) and Coot (12). The model was refined to an R_{cryst} value of 0.19 ($R_{free} = 0.23$), and contains 154 residues of hSpir1, 19 of hFmn2, and 85 waters. Almost all residues (99.4%) were in the favored region of the Ramachandran plot, and the remaining residues (0.6%) were in the allowed region. Crystallographic statistics are given in Table S2 and a representative region of electron density is shown in Fig. S4*B*.

Crystallization and Structure Determination of apo-Spir1 KIND. The apo-Spir1 KIND domain was prepared as described above for GST pull-down assays, with the exception that it was treated with recombinant His-TEV protease (3% wt/wt) for 16 hr at 4 °C prior to size-exclusion chromatography to remove the His_6-tag. Purified Spir1 KIND domain (7 mg/mL) was crystallized in 0.1 M Na-Hepes (pH 7.5), 5 mM TCEP, 150 mM NaCl, and 24% PEG 3350 using the hanging drop/vapor diffusion method in which 2 μL of protein were mixed with 2 μL of crystallization buffer. Larger single crystals for data collection were obtained by microseeding into hanging drops with the solution described above but with a lower concentration (20%) of PEG 3350. For data collection, crystals were stabilized in crystallization buffer supplemented with 20% ethylene glycol, mounted in Litholoops (Molecular Dimensions), and flash-frozen by plunging into liquid nitrogen. Diffraction data were collected at the Advanced Photon Source beamline ID24-E at 90 K. The crystals were of monoclinic space group $P2_1$ with four molecules in the asymmetric unit and diffracted anisotropically to 3.2 Å resolution. Moderate improvements in diffraction quality and resolution were obtained following 15 s of annealing and refreezing in the cryostream. The structure was determined by molecular replacement using the Spir1-KIND domain from the complex structure as a search model. The CCP4i suite (11) was used for all structure determination and refinement steps. The structure was refined to an R_{cryst} of 26.1% ($R_{free} = 31.5\%$) with data extending to 3.2 Å resolution. Most residues (88.4%) were in the favored region of the Ramachandran plot, and the remaining residues (11.6%) were in the allowed region. Molecules A and B were similarly well-ordered, whereas C and D were less well-defined in the electron density and had higher average temperature factors. Tight noncrystallographic restraints were maintained between chains A and B and between C and D throughout refinement. Crystallographic data collection and refinement statistics are outlined in Table S2 and a representative region of electron density for molecule A is shown in Fig. S4*C*.

GST Pull-Down Assays. GST-fused formin tail proteins were immobilized on glutathione sepharose beads and then resuspended in 25 mM Tris-HCl pH 8.0, 2 mM TCEP, 100 mM NaCl to make an approximately 50% (vol/vol) slurry, as described above. Equal portions of this slurry (containing 120 μg protein, approximated by Bradford assay) were mixed with a 2-fold molar excess of purified His_6-Spir1 KIND domain. The total volume was brought to 1 mL, and the mixture was nutated at 4 °C for 1 h. Beads were precipitated by centrifugation (600 × *g*, 1 min, 25 °C) and washed

three times with the same buffer. Beads were resuspended in a final volume of 1 mL and samples of both the input and pulled-down proteins were analyszed by standard gel electrophoresis.

Analytical Gel Filtration. Capu-CT (WT or I706A), Spir-NT, Dm-Spir-KIND, and actin were analyzed individually and in combination. For each run, 300 μL of sample was injected on a Superdex 200 10/300 GL column (GE) at a flow rate of 0.5 mL/min. Column buffer was actin G-buffer supplemented with 150 mM NaCl to mimic physiological ionic strength without inducing polymerization. Spir-NT, Capu-CT and actin were analyzed at the following final concentrations: 27.8 μM NT-Spir or Dm-Spir-KIND, 13.3 μM Capu-CT (WT or I706A), and 53.5 μM actin.

SEC-MALS. The purified human Fmn2-FH2C (aa 1267–1722) was mixed with purified Spir1-KIND at a 1:1.2 molar ratio. The complex was injected onto a Superdex 200 size-exclusion column attached to a GE AKTA purifier at a flow rate of 0.4 mL/min in buffer containing 20 mM Tris pH 8.0, 100 mM NaCl, 2 mM TCEP, and 1.7 μM purified Spir1-KIND. The eluted peak was analyzed using an in-line Wyatt miniDAWN TREOS multiangle light scattering instrument and Optilab rEX differential refractometer. Data were evaluated in ASTRA 5.3.4 software (Wyatt Technology).

Imaging of Spir and Capu in S2 Cells. The membrane-targeting sequence of Src64b was inserted at the 5′ end of mCherry in pValiump-mCherry-SpirD or pValiump-EGFP-CapuA (13). S2R+ insect cells (14) were cultured according to standard protocols and transfected with Spir and Capu constructs together with an actin-GAL4 driver using Effectene reagent (Qiagen). Transfected cells were incubated for 2 d at 20 °C, then fixed for 15 min in phosphate-buffered saline (PBS) containing 4% formaldehyde. Cells were washed twice with PBS and imaged for mCherry and GFP localization with a 100× lens on a Zeiss Observer Z1 microscope equipped with a Yokagawa CSU-X1 spinning disk confocal head and a QuantEM 512SC EMCCD camera (3I, Inc.). Figures show a single confocal slice; scale bar is 10 μm.

Filament Elongation Assays. Actin was purified from *Acanthamoeba castellani* as described (15) and stored in G-buffer (2 mM Tris-Cl, pH 8.0, 0.1 mM $CaCl_2$, 0.2 mM ATP, 0.5 mM TCEP, 0.04% sodium azide). F-actin seeds were prepared by polymerizing 5 μM actin at 25 °C for 1 h in KMEH (10 mM Na-Hepes pH 7.0, 1 mM EGTA, 50 mM KCl, 1 mM $MgCl_2$). The filaments were dispensed in 5 μL aliquots and allowed to reequilibrate for 2–3 h at 25 °C. Based on the elongation rate of 0.5 μM monomeric actin in the presence of seeds, as well as the kinetic rate constants for Mg-ATP-G-actin addition/dissociation at the barbed end ($k_+ = 11.6\ \mu M^{-1}\ s^{-1}$ and $k_- = 1.4\ s^{-1}$) (16), we calculated a barbed end concentration of approximately 50 pM in these assays. Prior to adding capping protein, Capu-CT, Capu-CT plus Dm-Spir-KIND, Dm-Spir-KIND, or buffer alone were incubated with filaments for 3 min at 25 °C. During this incubation time, monomeric actin was converted to Mg-G-actin as described for nucleation assays. Using a cut pipette tip to prevent shearing, polymerization buffer was added to Mg-G-actin and then mixed with seeds plus additional protein components. The slope of the pyrene fluorescence trace between 200 and 500 s was considered the elongation rate.

Filament Annealing. Actin filaments were polymerized in KMEH and stabilized with equimolar phalloidin labeled with either AlexaFluor488 or AlexaFluor647. The two colors of actin were mixed at 0.5 μM and sheared by five passes through a 27G1/2 needle. After shearing, protein or buffer control was added and mixed by gently pipetting the whole solution twice. A sample was diluted to 2 nM and spotted on poly-L-lysine coated coverslips immediately after shearing, to ensure uniform breakage, and after 30 min, to assess the extent of reannealing. To assess the importance of order of addition, "Capu-CT and KIND" indicates that these proteins were mixed before adding them to actin, whereas "Capu-CT then KIND" indicates that Capu-CT was present during shearing and Dm-Spir-KIND was subsequently added. Final concentrations were 10 nM Capu-CT and 1 μM Dm-Spir-KIND.

Miscellaneous Methods. Point-mutations in Spir1, Fmn2, Spir, or Capu expression constructs were engineered using Quikchange site-directed mutagenesis according to manufacturer's instructions (Agilent Technologies). Mutations in several pValium transgenic constructs were made by overlapping extension PCR mutagenesis of the insert region and subcloning back into pValium (17).

1. Pechlivanis M, Samol A, Kerkhoff E (2009) Identification of a short Spir interaction sequence at the C-terminal end of formin subgroup proteins. *J Biol Chem* 284:25324-25333.
2. Vinson VK, De La Cruz EM, Higgs HN, Pollard TD (1998) Interactions of *Acanthamoeba profilin* with actin and nucleotides bound to actin. *Biochemistry* 37:10871–10880.
3. Quinlan ME, Hilgert S, Bedrossian A, Mullins RD, Kerkhoff E (2007) Regulatory interactions between two actin nucleators, Spire and Cappuccino. *J Cell Biol* 179:117–128.
4. Quinlan ME, Kerkhoff E (2008) Actin nucleation: Bacteria get in-Spired. *Nat Cell Biol* 10:13–15.
5. Dahlgaard K, Raposo AASF, Niccoli T, Johnston DS (2007) Capu and Spire assemble a cytoplasmic actin mesh that maintains microtubule organization in the Drosophila oocyte. *Dev Cell* 13:539–553.
6. Quinlan ME, Heuser JE, Kerkhoff E, Mullins RD (2005) Drosophila Spire is an actin nucleation factor. *Nature* 433:382–388.
7. Bosch M, et al. (2007) Analysis of the function of Spire in actin assembly and its synergy with formin and profilin. *Mol Cell* 28:555–568.
8. Ito T, et al. (2011) Human Spire interacts with the barbed end of the actin filament. *J Mol Biol* 408:18–25.
9. Otwinowski Z, Minor W (1997) Processing of X-ray diffraction data collected in oscillation mode. *Macromolecular Crystallography, Pt A* 276:307–326.
10. Morris RJ, Perrakis A, Lamzin VS (2003) ARP/wARP and automatic interpretation of protein electron density maps. *Methods Enzymol* 374:229–244.
11. Potterton E, Briggs P, Turkenburg M, Dodson E (2003) A graphical user interface to the CCP4 program suite. *Acta Crystallogr D Biol Crystallogr* 59:1131–1137.
12. Emsley P, Cowtan K (2004) Coot: Model-building tools for molecular graphics. *Acta Crystallogr D Biol Crystallogr* 60:2126–2132.
13. Ni J-Q, et al. (2008) Vector and parameters for targeted transgenic RNA interference in *Drosophila melanogaster. Nat Methods* 5:49–51.
14. Cherbas L, Cherbas P (1998) *Drosophila: A Practical Approach* (Oxford, IRL Press). 2nd Ed.
15. Zuchero JB (2007) In vitro actin assembly assays and purification from Acanthamoeba. *Methods Mol Biol* 370:213–226.
16. Pollard TD (1986) Rate constants for the reactions of ATP- and ADP-actin with the ends of actin filaments. *J Cell Biol* 103:2747–2754.
17. Ho SN, Hunt HD, Horton RM, Pullen JK, Pease LR (1989) Site-directed mutagenesis by overlap extension using the polymerase chain reaction. *Gene* 77:51–59.

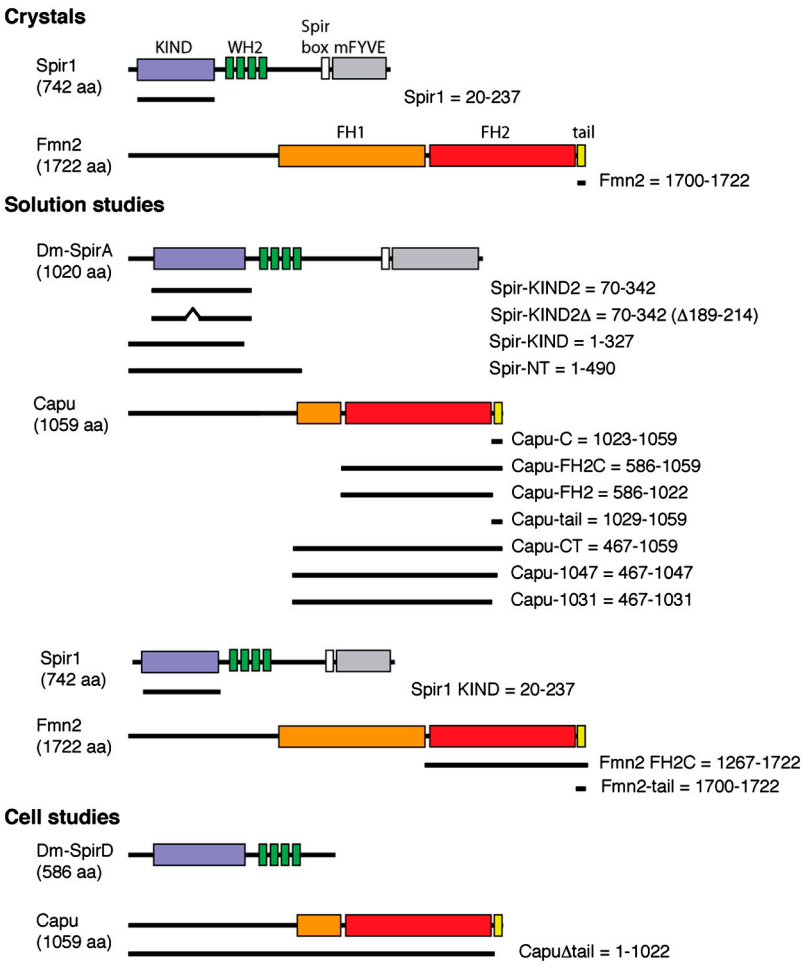

Fig. S1. Diagrams of constructs used in this paper. Full-length constructs and relevant domains are indicated at the top of each section. Below are lines depicting shorter constructs and the residues they encompass are indicated to the right of each line. Major domains indicated are: KIND, kinase noncatalytic C-lobe domain (blue); WH2, Wiscott-Aldrich homology-2 motif (green); Spir box (white); mFYVE, modified Fab1/YOTB/Vac1/EEA1 zinc-binding domain (gray); FH1, formin homology-1 (orange); FH2, formin homology-2 (red); tail (yellow). Affinity tags used (GST or His_6) are indicated in the text.

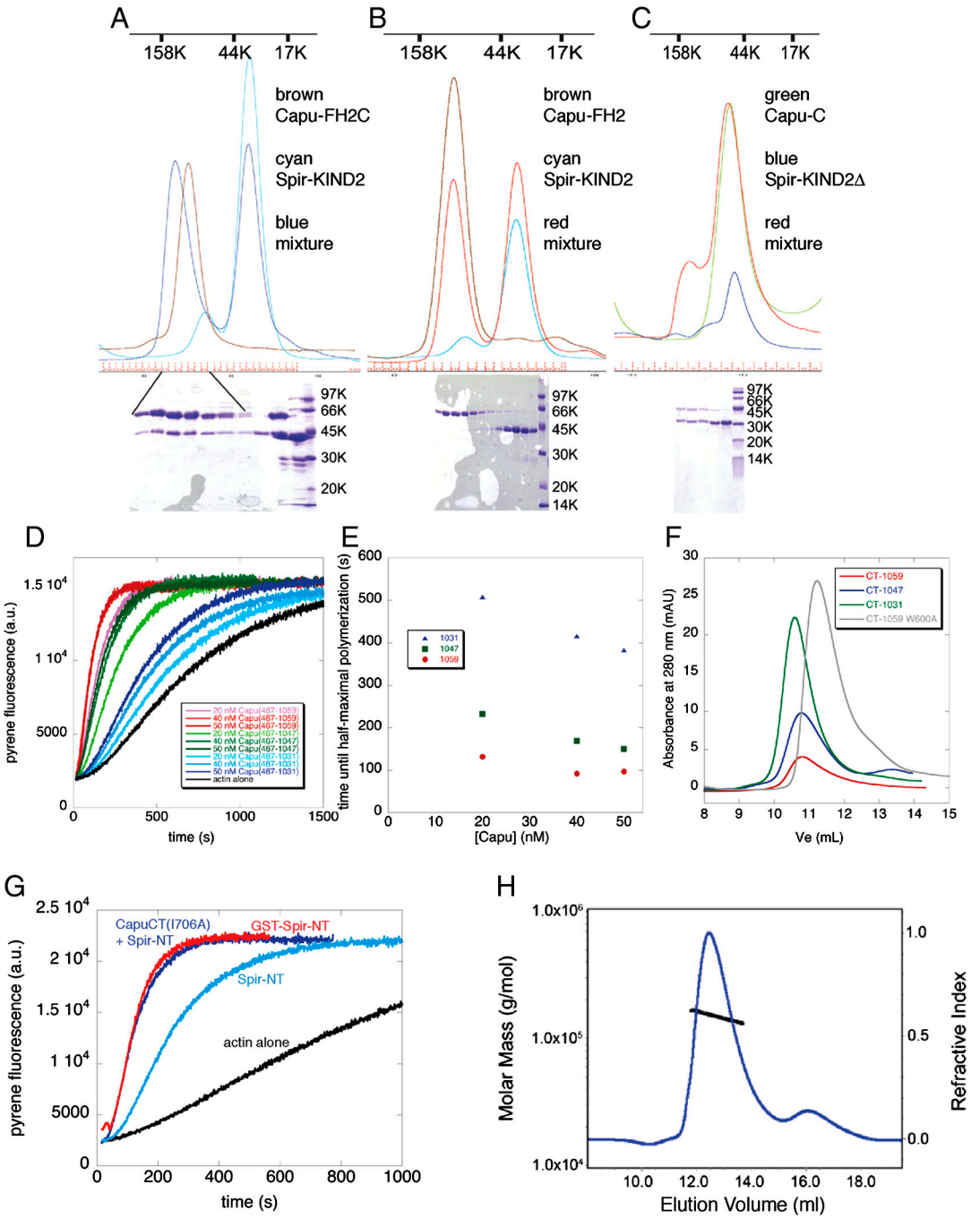

Fig. S2. The Capu-tail interacts with Spir. Analytical gel-filtration of the Spir and Capu fragments shows that the tail is necessary and sufficient for KIND binding. (*A*) Capu-FH2C contains the tail domain and coelutes with Dm-Spir-KIND. (*B*) The Capu-FH2 domain, lacking the tail, does not coelute with Dm-Spir-KIND. (*C*) A fusion protein containing GST plus the Capu-tail domain, Capu-C, coelutes with KIND. (*D*) Titrations of Capu-CT and two truncations show that actin assembly kinetics are dramatically affected by the loss of residues beyond the FH2 domain. Both lag times and time to half-maximal polymerization are increased with severity corresponding to the amount of the C-terminus removed. (*E*) Comparison of time to half-maximal polymerization at different concentrations of Capu constructs shown in (*D*). (*F*) Analytical gel-filtration of the truncated Capu-CT constructs. Capu-1031 and Capu-1047 elute at a volume expected for dimeric, full-length Capu-1059. A predicted monomeric mutant of Capu-1059 [W600A, analogous to Bni1 W1363 (1, 2) and human Daam1 W615 (3)] elutes later. Proteins were injected onto a Superdex 200 size column in buffer containing 50 mM Na-Hepes pH 7.0, 150 mM NaCl, 1 mM DTT. Protein concentrations were 8–14 μM monomer. (*G*) Actin polymerization stimulated by 200 nM of GST-Spir-NT (an obligate dimer) is much faster than when 200 nM Dm-Spir-NT (presumed monomer) is added. Strikingly, the rate of actin polymerization in the presence of 200 nM GST-Spir is very similar to the enhanced rate seen when nucleation-dead Capu-CT(I706A) is added to 200 nM Spir-NT, supporting our hypothesis that enhancement of nucleation is due to dimerization. (*H*) SEC-MALS analysis of human Fmn2-FH2C in complex with the Spir1 KIND domain. Molar mass (black trace, MM) and refractive index (blue trace, RI) are plotted versus elution volume from a Superdex 200 size-exclusion column for the complex. Derived molar mass for the complex is 150 kDa, in good agreement with the predicted molecular weight for a 2:2 complex (146 kDa). Note that the size-exclusion chromatography was carried out with 1.7 μM Spir1-KIND domain in the gel-filtration buffer (see *SI Methods*).

1 Moseley JB, Goode BL (2005) Differential activities and regulation of *Saccharomyces cerevisiae* formin proteins Bni1 and Bnr1 by Bud6. *J Biol Chem* 280:28023–28033.
2 Xu Y, et al. (2004) Crystal structures of a Formin Homology-2 domain reveal a tethered dimer architecture. *Cell* 116:711–723.
3 Lu J, et al. (2007) Structure of the FH2 domain of Daam1: Implications for formin regulation of actin assembly. *J Mol Biol* 369:1258–1269.

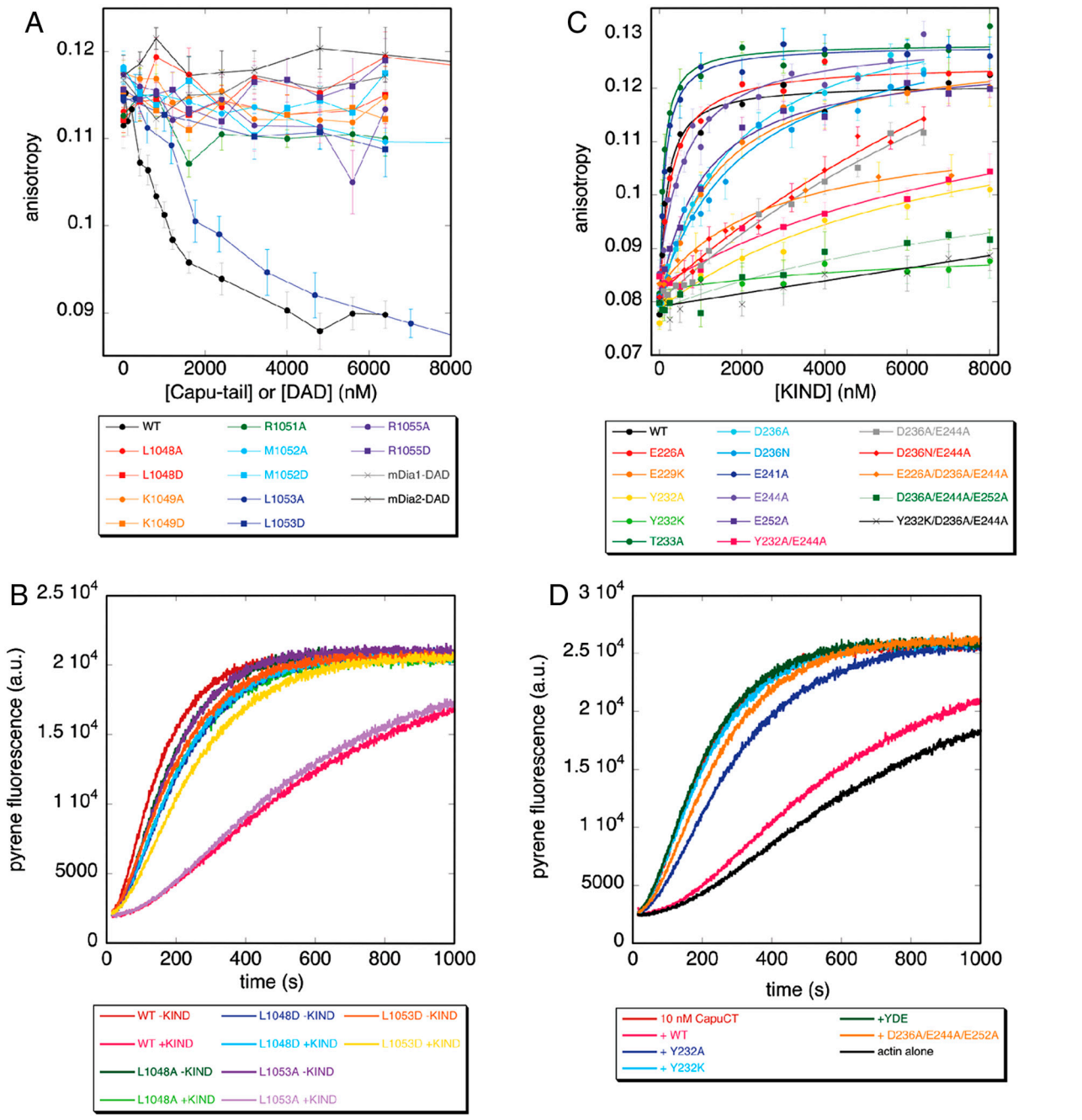

Fig. S3. Capu-tail and Dm-Spir-KIND mutatgenesis. (*A*) Competition anisotropy with all Capu-tail mutations made. We mixed 10 nM Capu-tail-AlexaFluor488 and 600 nM Dm-Spir-KIND with varying concentrations of unlabeled Capu-tail wild-type (WT) and mutants. Single point-mutations of all conserved residues tested abolished KIND/tail binding. Neither mDia1-DAD nor mDia2-DAD binds to Dm-Spir-KIND. (*B*) Representative pyrene assays from Fig. 3*D*. KIND no longer inhibits Capu-CT when conserved residues are mutated (e.g., L1048). When poorly conserved L1053 is mutated to alanine, KIND inhibits L1053A Capu-CT as well as KIND inhibits WT Capu-CT (pink and light purple traces). (*C*) Polarization anisotropy of 10 nM Capu-tail-AlexaFluor488 and increasing concentrations of Spir-KIND domain, WT or with indicated point-mutations. Error bars represent SD. (*D*) Strong KIND mutations (as determined by polarization anisotropy) fail to inhibit actin assembly by Capu-CT.

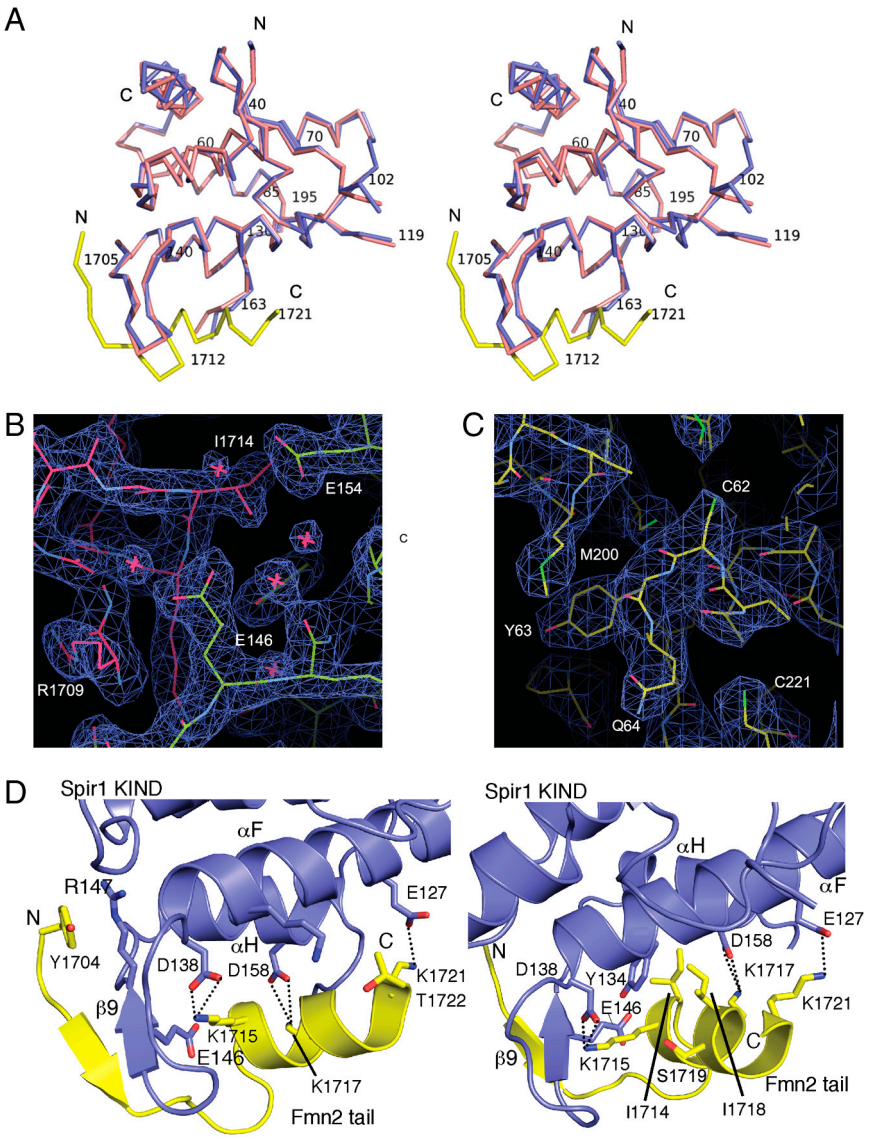

Fig. S4. Structure of the apo-Spir-KIND domain. (*A*) Stereo diagram comparing apo-Spir-KIND with the Spir-KIND/tail complex. A Cα backbone trace of the unliganded KIND domain structure (pink) is superimposed on that of the Spir-KIND/tail complex (colored blue and yellow as in Fig. 1*D*). N- and C-termini and selected residues are labeled. (*B*) Representative electron density for Spir-KIND/Fmn2-tail structure. The 2Fo-Fc map is contoured at 1.2σ. The KIND domain is shown with carbon atoms colored green, the Fmn2 tail with carbon atoms colored pink. The pink "stars" are ordered water molecules. (*C*) Electron density for apo-Spir-KIND structure. The 2Fo-Fc map corresponding to a region of molecule A is contoured at 1.2σ. (*D*) Detailed views of the Spir1/Fmn2 peptide interface. Selected main chain and side chain atoms are drawn in stick representation. Hydrogen bonds are illustrated with dashed black lines.

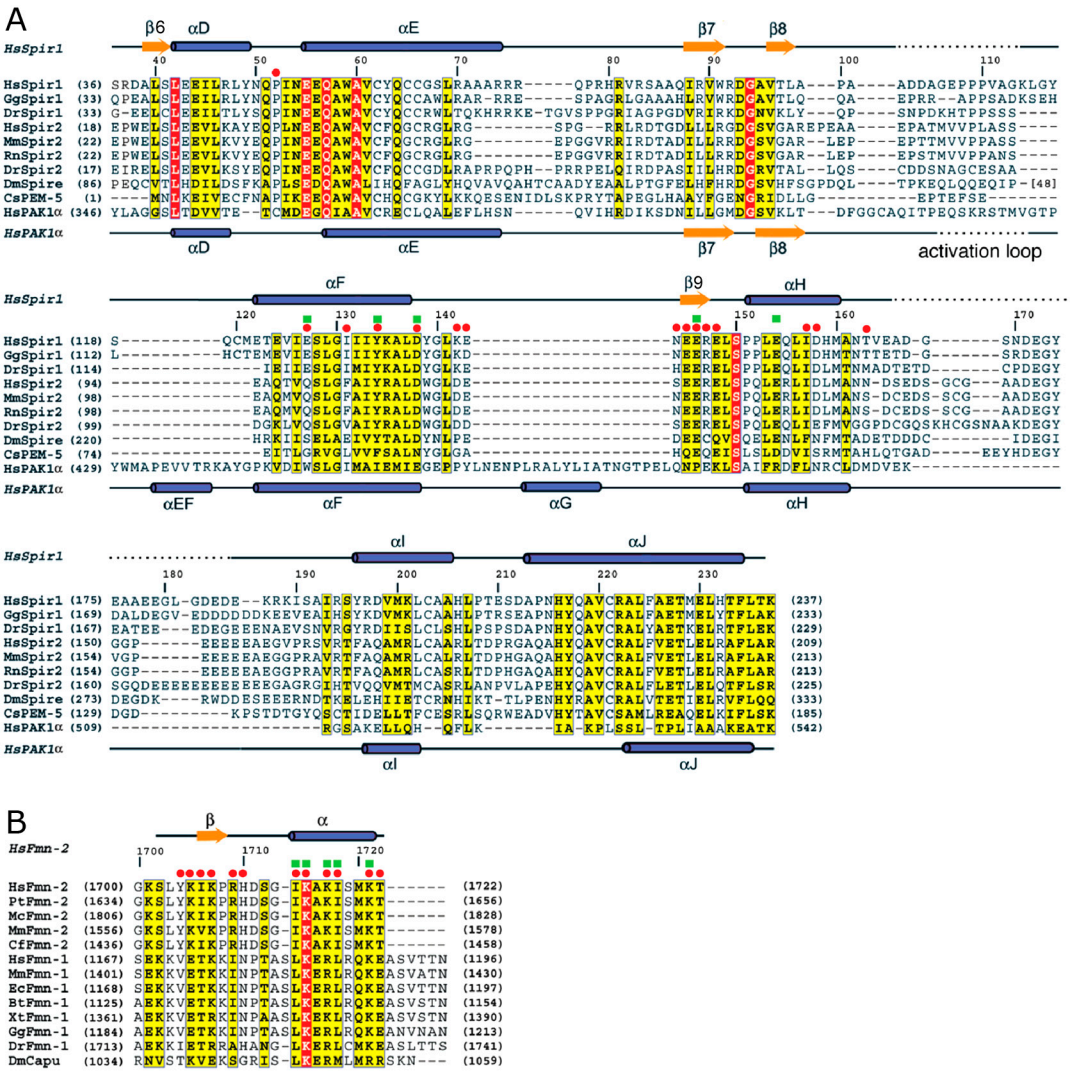

Fig. S5. Structure-based sequence alignments of Spir and Fmn-family members. (*A*) Sequences of the KIND domain of several Spir family proteins and the protein kinase PAK1 are aligned based on the structural superposition of the Spir1 KIND domain and PAK1 kinase. Secondary structure elements of human Spir1 are illustrated above the alignment, and those of PAK1 are illustrated below the alignment using kinase nomenclature for both. Unstructured regions are shown with dashed lines. Note that the long, unstructured loop connecting strand β8 and helix αF in the KIND domain is topologically equivalent to the activation loop of protein kinases. Strands β6 and β9 are not present in PAK1. A 48-residue insertion ("48") in *Drosophila* Spire was omitted for clarity. Yellow boxes indicate regions of sequence conservation, and red boxes indicate absolute conservation. Red circles indicate residues located in the binding interface, and green squares indicate residues that when mutated were found to disrupt Spir1/Fmn2 and/or Spir/Capu interactions. Spir sequences include: Hs, *Homo sapiens*; Gg, *Gallus gallus*; Dr, *Danio rerio*; Mm, *Mus musculus*; Rn, *Rattus norvegicus*; Dm, *Drosophila melanogaster*; Cs, *Ciona savignyi*. (*b*) Comparisons of Fmn-family tail sequences from various organisms. Aligned sequences are presented with the residue numbering and the secondary structural elements of human (*Hs*) Fmn2 above the alignment. Coloring and symbols are as described for panel *A*. Sequences (in addition to abbreviations from panel *A*) are from: Pt, *Pan troglodytes*; Mc, *Macaca mulatta*; Cf, *Canis familiaris*; Ec, *Equus caballus*; Bt, *Bos taurus*; Xt, *Xenopus tropicalis*.

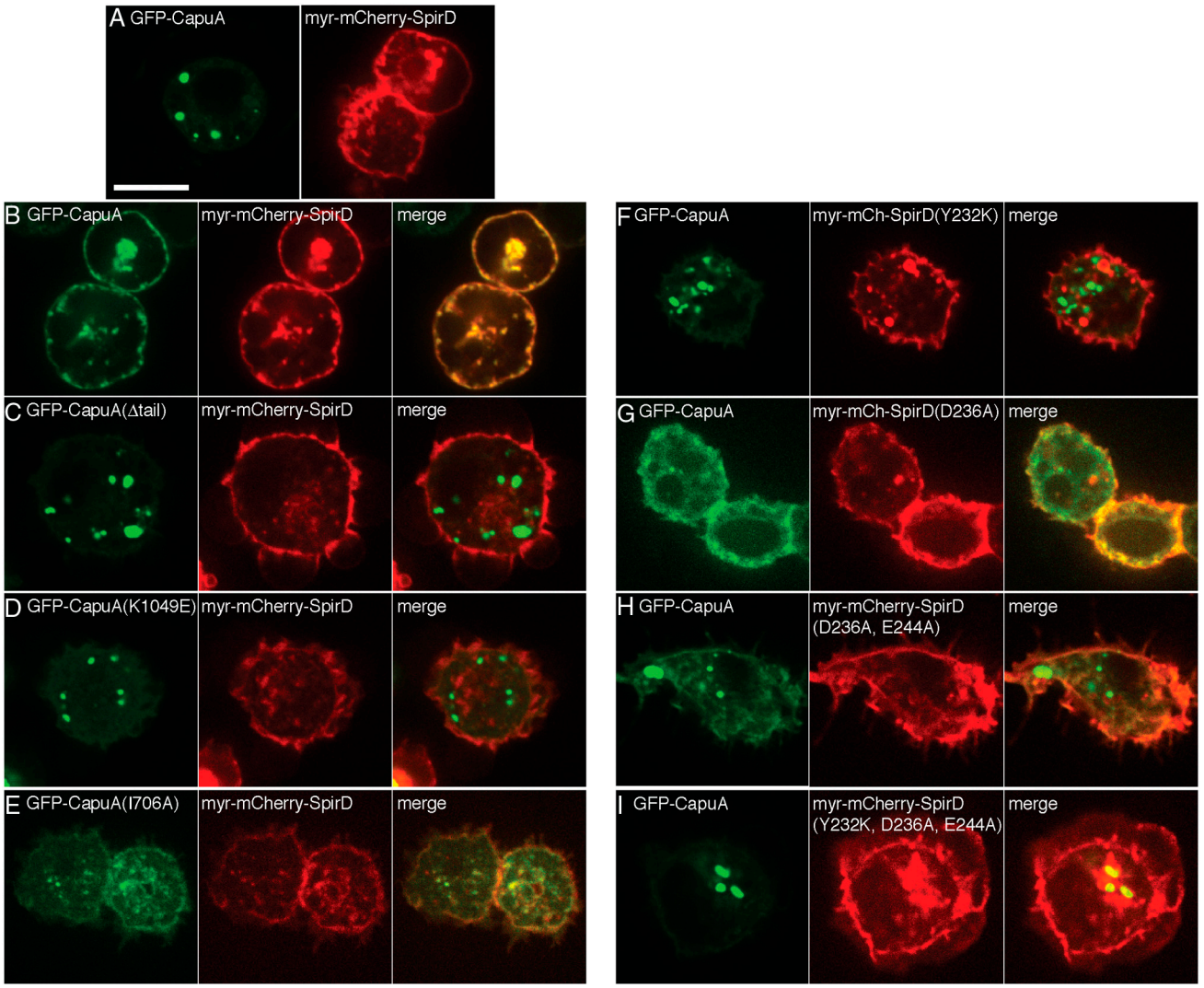

Fig. S6. In vivo requirements for colocalization of Capu and Spir. (*A*, *B*, *D*, and *F*) WT CapuA-GFP and WT myr-mCherry-SpirD, CapuA(K1049E), and SpirD (Y232K) are the same as in Fig. 4 and are shown again for comparison. WT CapuA-GFP and WT myr-mCherry-SpirD are expressed (*A*) individually or (*B*) together in S2 cells. (*C*, *D*) Deleting the tail (Δtail) or mutating a single conserved residue (K1049E) abolishes colocalization. CapuA is localized in these cells as if it were expressed alone [compare to (*A*)]. (*E*) Nucleation activity of Capu is not necessary for colocalization [CapuA(I706A)]. [*F*–*I*] Amount of colocalization corresponds to binding affinity measured in vitro for KIND mutants. (*F*) A strong mutation in SpirD-KIND (Y232K) does not colocalize with Capu. (*G*) A weak mutation (D236A) pulls CapuA out of puncta. (*H*) A double mutant in SpirD-KIND (D236A, E244A) that decreases binding affinity relative to D236A alone is partially compromised in pulling CapuA away from puncta. (*I*) A triple mutant (Y232K, D236A, E244A) with undetectable binding in vitro fails to pull CapuA away from cytoplasmic puncta. Scale bar is 10 μm.

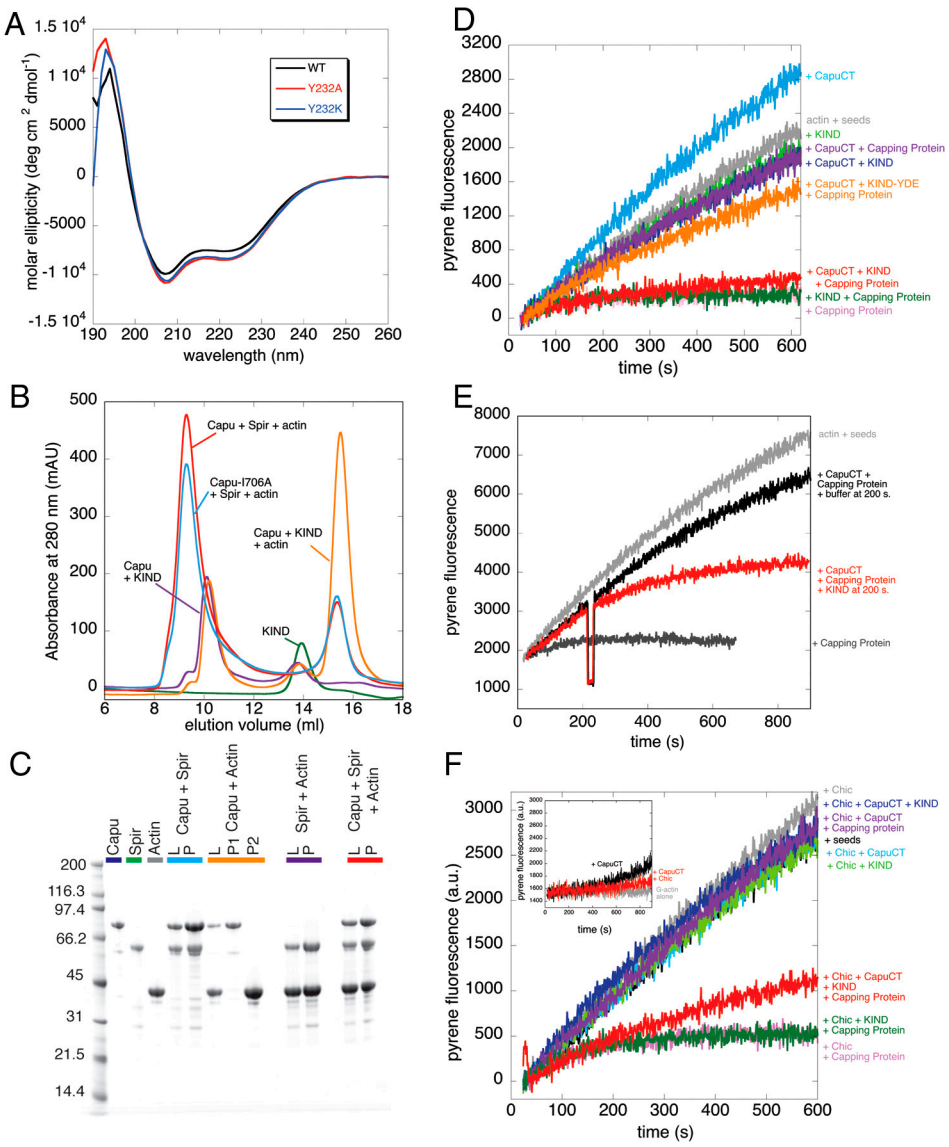

Fig. S7. The KIND domain competes with filament barbed ends for Capu-CT binding. (*A*) Circular dichroism of Dm-Spir-KIND. Mutations at Y232 do not grossly disrupt the Dm-Spir-KIND structure. Data are the average of three runs. Conditions: 50 mM potassium phosphate pH 7.4, 6–10 μM KIND. (*B*) Analytical gel-filtration of Capu-CT, Spir-NT, and actin demonstrates that these three proteins form a stable complex (red trace, repeat of data from Fig. 5*C*). Gel-filtration of Capu-CT, KIND and actin demonstrates that Spir-WH2 domains are necessary for actin stability in this complex (orange trace). Gel-filtration of Spir-NT and Capu-CT(I706A) shows that Spir-WH2 domains are sufficient for actin stability in the complex (light blue). For each run, 300 μL of sample was injected on a Superdex 200 10/300 GL column (GE). Column buffer was actin G-buffer supplemented with 150 mM NaCl. Proteins were mixed at the following concentrations: 27.8 μM Dm-Spir-KIND, 27.8 μM Spir-NT, 13.3 μM Capu-CT, 13.3 μM Capu-CT(I706A) and 53.5 μM actin. (*C*) SDS-PAGE analysis of column load (L) and peak (P) samples from analytical gel-filtration of the Capu–Spir–actin complex in Fig. 5*C*. For each individual protein, the load sample is shown. The peak sample refers to the largest MW (earliest elution volume) observed in the elution profile. For the mixture of Capu-CT and actin, two peak samples were analyzed: P1 corresponds to $V_e = 10.6$ mL (Capu-CT alone) and P2 corresponds to $V_e = 15.3$ mL (actin alone). (*D*) Elongation assays (representative pyrene traces for Fig. 5*A*) show that Capu-CT protects barbed ends of growing filaments from capping protein but cannot do so in the presence of KIND. Capu-CT (light blue trace) modestly increases the assembly rate from preformed seeds compared to the G-actin plus seeds (gray trace), this increase is likely due to a low level of nucleation (see below). (*E*) Elongation assays with the order of addition altered show that KIND can knock Capu-CT off the end of growing filaments. KIND or buffer control is added after elongation is initiated. (*F*) The slight increase in elongation rate in the presence of Capu-CT (panel *D* light blue vs. gray trace) is caused by nucleation. (See *SI Discussion* for further analysis.) There is a small enhancement of actin assembly by Capu-CT in reactions mimicing the elongation assays (0.5 μM actin) but lacking preformed seeds (*Inset*). In the presence of profilin (Chic = Drosophila profilin), the assembly rate from seeds is the same with or without Capu-CT (light blue vs. gray traces). Profilin does not alter the interactions between the KIND domain, Capu-CT and barbed ends.

Table S1. Binding affinities measured for spire KIND domain mutants

Mutant	K_d for Capu-tail-AlexaFluor488 (nM)*	Anisotropy of Capu-tail-AlexaFluor488 in 6.4 μM Dm-Spir-KIND	Spir1 residue #
WT	140 ± 20 (290 ± 60[†])	0.121	—
E226A	260 ± 40	0.123	S148 (E127)[§]
E229K	1300 ± 300	0.120	I131 (E127)[§]
Y232A	n/d[‡]	0.102	Y134
Y232K	n/d[‡]	0.086	Y134
T233A	90 ± 10	0.127	K135
D236A	1700 ± 200	0.123	D138
D236N	2100 ± 4	0.123	D138
E241A	110 ± 10	0.128	E143
E244A	600 ± 100	0.130	E146
E252A	1000 ± 200	0.119	E154
D236A/E244A	n/d[‡]	0.112	—
D236N/E244A	n/d[‡]	0.114	—
Y232A/E244A	n/d[‡]	0.103	—
E226A/E244A/E252A	2800 ± 700	0.104	—
D236A/E244A/E252A	n/d[‡]	0.093	—
Y232K/D236A/E244A	n/d[‡]	0.088	—

*K_d derived from the anisotropy of 10 nM of Capu-tail-AlexaFluor488 at varying concentrations of WT or mutant Dm-Spir-KIND, as indicated.

[†]The K_d reported in the text (290 nM) was derived from the anisotropy of 10 nM Capu-tail-AlexaFluor488, 800 nM KIND, and varying concentration of unlabeled Capu-tail to control for the effect of the fluorescent dye on the binding affinity.

[‡]The text n/d represents "not determined" because error in fit >25% of derived K_d value and plateau not reached at 6.4 μM KIND. Best estimates range from 6–16 μM. Visual inspection (see Fig. S3) indicates binding in order of increasing K_d: D236N/E244A≅D236A/E244A > E226A/D236A/E244A ≥ Y232A≅Y232A/E244A > D236A/E244A/E252A ≥ Y232K≅Y232K/D236A/E244A.

[§]*Drosophila* KIND does not contain an obvious amino acid correlate of E127, but the contacts made by E127 may be fulfilled by E226 or E229.

Table S2. Crystallographic data collection and refinement statistics*

	Spir-KIND/Fmn2 Tail Complex (MIR)			Spir-KIND
	Native	$(CH_3CH_2)HgPO_4$	K_2PtCl_4	Native
Data collection				
Space group	$P4_32_12$	$P4_32_12$	$P4_32_12$	$P2_1$
Cell dimensions				
a, *b*, *c* (Å)	66.4, 66.4, 116.4	66.3, 66.3, 116.2	66.5, 66.5, 116.6	73.3, 66.3, 100.9
α, β, γ (°)	90, 90, 90	90, 90, 90	90, 90, 90	90, 103, 90
Resolution (Å)	45–2.2 (2.24–2.2)	38–2.45 (2.49–2.45)	40–2.35 (2.39–2.35)	41–3.2 (3.26–3.2)
R_{merge}[†]	0.081 (0.358)	0.064 (0.354)	0.056 (0.267)	0.061(39.9)
$I/\sigma I$	16.1 (1.58)	17.6 (2.36)	14.2 (3.10)	14(2.0)
Completeness (%)	95.5 (70.6)	97.8 (83.2)	97.2 (94.4)	94.3(82.0)
Redundancy	4.1 (1.8)	5.8 (3.0)	3.0 (2.6)	5.3(5.0)
Refinement				
Resolution (Å)	80–2.2			25–3.2
No. reflections	12200			14116
R_{work}/R_{free}[‡]	0.19/0.23			0.261/0.315
No. atoms	1470			4850
Protein	1385			4845
Water	85			5
Average *B*-factors				
Protein	32.8			99.7
Water	42.1			53.1
R.m.s deviations				
Bond lengths (Å)	0.0122			0.012
Bond angles (°)	1.304			1.33

*Statistic for highest resolution shell is shown in parentheses.

[†]Rmerge $= \sum |I_i - < I >| / \sum I_i$, where I_i is the *i*th measurement of the intensity of an individual reflection or its symmetry-equivalent reflections and <I > is the average intensity of that reflection and its symmetry-equivalent reflections.

[‡]Rwork $= \sum ||Fobs| - |Fcalc|| / \sum |Fobs|$ for all reflections and *R*free $= \sum ||Fobs| - |Fcalc|| / \sum |Fobs|$, calculated on the 5% of data excluded from refinement.